ISSN: 2710-0723

High-Temperature Regulation of Manganese Oxide Hybrid for Efficient Alkaline Oxygen Evolution Reaction

Tao Feng, Zonglong Lu

College of Material, Chemistry and Chemical Engineering, Hangzhou Normal University, Hangzhou 311121, Zhejiang, China

Abstract

Manganese-based oxides with diverse oxidation states, are promising electrochemical catalysts. In this work, we fabricated a novel hybrid electrocatalyst by integrating Mn_2O_3 and α-MnO_2 on carbon paper (CP) using a two-step electrodeposition process, followed by annealing treatments at various temperatures. Notably, the hybrid electrocatalyst demonstrated significant performance enhancements compared to individual manganese oxides. In 1 M KOH electrolyte, the hybrid electrocatalyst displayed superior oxygen evolution reaction (OER) performance, requiring only a low overpotential of 290 mV to reach 10 mA cm^{-2}. This electrocatalyst also exhibited excellent stability, maintaining performance over 12 hours. The results suggest that the synergistic combination of Mn_2O_3 and MnO_2 plays a crucial role in enhancing OER performance.

Keywords

Manganese-based Oxides; Electrocatalyst; Oxygen Evolution; Alkaline Electrolyte.

1. Introduction

The energy crisis resulting from the excessive extraction and consumption of fossil fuels, coupled with the escalating severity of climate change, has emerged as two prominent challenges in contemporary human development[1,2]. Hydrogen could replace fossil fuels in clean energy, and increasing hydrogen production through water electrolysis is a promising sustainable pathway. IrO_2 and RuO_2 exhibit exceptional electrocatalytic activity in OER catalysts.[3,4] Their exorbitant expense and rarity impede and confine their large-scale deploymen. Mn2O3, notable for their low cost, abundance, structural flexibility, are highly effective electrochemical catalysts[5,6]. However, Mn_2O_3 encounters several challenges. Under electrochemical conditions, Mn_2O_3 may undergo partial dissolution or phase transitions, which compromise its long-term stability, result in a high initial potential, and restrict its performance in oxygen evolution reactions (OER)[7].

In this work, we developed a hybrid manganese-based. Mn2O3 was modified by adjusting different oxidation states of Mn and superimposing different oxides at high temperature. The results indicate that the newly synthesized hybrid manganese-based oxides exhibit enhanced stability and significantly improved electrochemical performance in alkaline environments.

2. Synthesis of Hybrid Manganese-based

The preparation process was shown in Figure S1, disperse 36.75g of manganese acetate in 500ml of water, stir evenly to dissolve into a 0.3M solution, and perform electrodeposition using a standard three electrode system. At a constant voltage of 1.8V relative to the Ag/AgCl reference electrode, ultrasonic deposition was carried out for 300s and then dried in a 50 ℃ oven. After annealing at 500 ℃ for 10min, the crystalline phase formed is referred to as Mn2-CP. Using the same 1.8V voltage, ultrasonic electrodeposition was repeated for 300s and

ISSN: 2710-0723

annealed in air at 300 ℃ for 20min to obtain the crystalline phase (when this method is used alone, the sample is recorded as Mn1-CP), which was recorded as Mn12-CP.

3. Results and Discussion

Scanning electron microscopy (SEM) examined the surface morphology of annealed Mn-based oxide nanostructures. Figure 1a shows Mn1-CP. A distinct layered structure with a rough, bubble-like surface appears on the carbon fibers. Figure 1b shows Mn2-CP. Figure 1c shows Mn12-CP at 1 μm magnificatio, increase its specific surface area, may lead to the improving electrochemical performance. Elemental mapping analyzed Mn and O distribution. Figure 1d shows the Mn12-CP sample at 10 μm, with Mn and O regions visible in Figures 1e and 1f. This confirms the manganese-based oxides form a layered structure around the carbon paper.

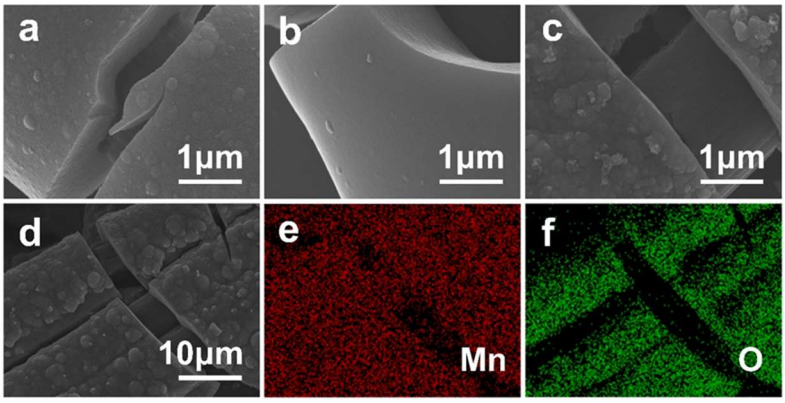

Figure 1. (a) Mn1-CP, (b) Mn2-CP, (c) Mn12-CP, (d) Mn12-CP in 10μm, (e) Mn elements regions, (f) O elements regions.

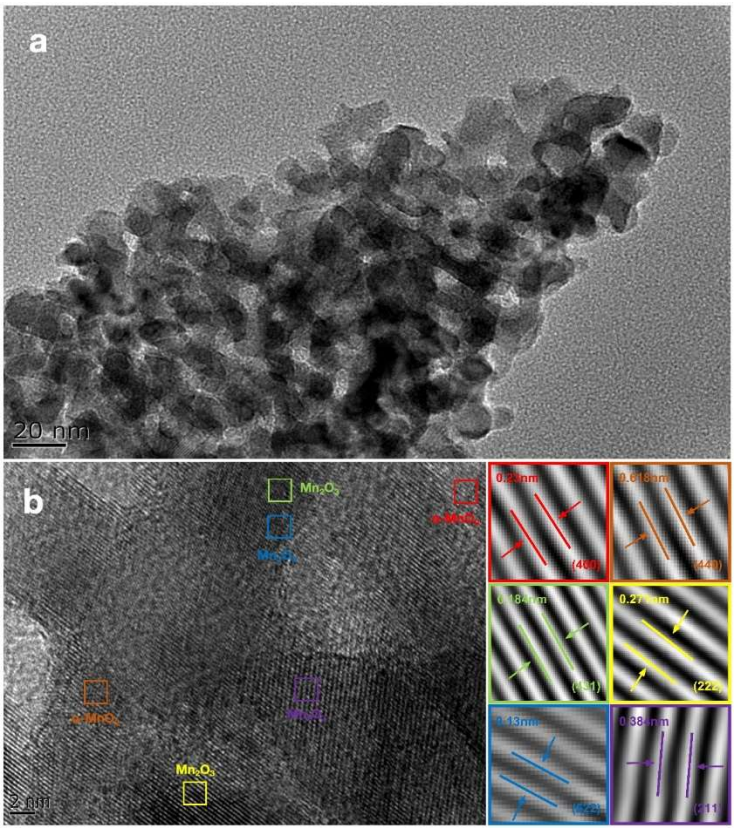

Figure 2. (a) TEM, (b) HRTEM image of Mn12-CP.

ISSN: 2710-0723

Figure 2a shows a TEM micrograph with substantial spherical aggregation, consistent with SEM. High-resolution transmission electron microscopy (HR-TEM) elucidated the microstructure of the doped material. Figure 2b shows HR-TEM images of Mn12-CP with lattice stripes at 0.23 nm and 0.168 nm for α-MnO2 (ICDD PDF#00-044-0141). Lattice fringes at 0.184 nm, 0.271 nm, 0.384 nm, and 0.13 nm correspond to the (431), (222), (622), and (211) planes of Mn2O3 (JCPDS 71-0636). This indicates that Mn2O3 and α-MnO2 co-exist.

As shown X-ray diffraction in Figure 3a, diffraction peaks are observed at 2θ = 32.929°, 55.140 °, 23.1 °, 38.2 °, 65.7 °, 49.314 ° and 45.133°. These can be assigned to reflections of (222), (440), (211), (400), (622), (431), and (332), correspondingly. Figure 3a shows this peak matching the standard Mn2O3 cubic phase (JCPDS 71-0636)[8,9]. The peak at 2θ = 32.9° with a D-spacing of 0.27 nm matches the substrate material. Diffraction peaks at 2θ = 26.611° and 54.801° correspond to (111) and (222), aligning with standard Graphite C (JCPDS 75-2078). As shown in Figure 3b,Diffraction peaks at 2θ = 37.522°, 41.968°, 60.274°, and 69.711° correspond to (211), (301), (521), and (541). Mn2-CP is identified as α-MnO2, matching standard α-MnO2 (ICDD PDF#00-044-0141). As shown in Figure 3c, diffraction peaks are evident at 2θ = 32.929°, 55.140°, 23.1°, 38.2°, 65.7°, 49.314°, and 45.133°. Same as standard Graphite C (JCPDS 75-2078). Potentially due to Mn1-CP overshadowing the peak value of Mn2-CP in the figure, This figure shows the XRD curves of Mn2O3 and standard Mn2O3.

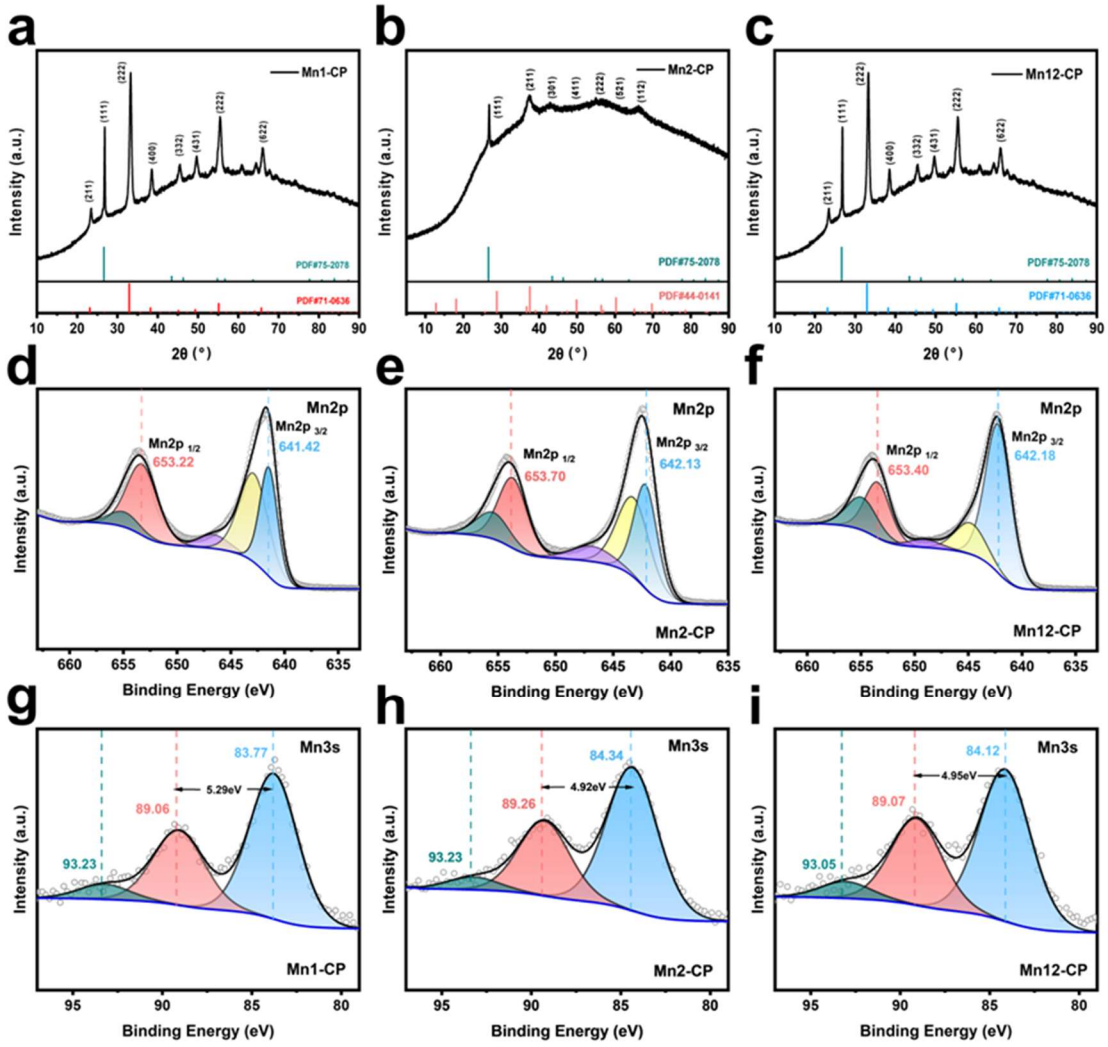

Figure 3. (a) XPS of Mn1-CP ,(b) XPS of Mn2-CP, (c) XPS of Mn12-CP,(d)Mn1-CP 2p, (e)Mn1-CP 3s, (f)Mn2-CP 2p, (g)Mn2-CP 3s, (h)Mn12-CP 2p, (i)Mn12-CP 3s

ISSN: 2710-0723

X-ray photoelectron spectroscopy (XPS) revealed the oxidation state of manganese in oxide deposits. Figure 3d and 3g show Mn1-CP Mn2p peaks at 641.42 and 653.22 eV, corresponding to Mn2p3/2 and Mn2p1/2, with an 11.8 eV spin energy gap, confirming Mn2O3[10,11]. The Mn3s spin energy gap (5.29 eV) and expected peak splitting confirm the identification of Mn2O3[12], suggesting that Mn is predominantly present on the catalyst's surface in the Mn3+ state. Figure 3e and Figure 3h demonstrate that upon annealing Mn2-CP, two peaks at binding energies of 642.13 and 653.7 eV are discernible in its XPS spectrum. The binding energy indicates Mn2-CP has a higher valence state than Mn1-CP. Since Mn1-CP corresponds to Mn(II) and Mn(III), Mn2-CP is likely Mn(IV), confirming MnO2 via XRD analysis. The 4.92 eV spin energy gap of Mn3s, matching the expected peak splitting, supports the identification of MnO2. Mn is likely present on the catalyst surface as Mn4+. Figure 3f and 3i show that in Mn12-CP, the spectrum has binding energies of 642.18 eV and 653.4 eV for Mn2p3/2 and Mn2p1/2, respectively. The 4.95 eV spin energy gap suggests Mn3s is in a complex state, neither Mn3+ nor Mn4+. This indicates a complex state, confirming that Mn12-CP has a valence state between Mn(III) and Mn(IV), leading to a new oxide film. The full spectrum is shown in Figure S4.

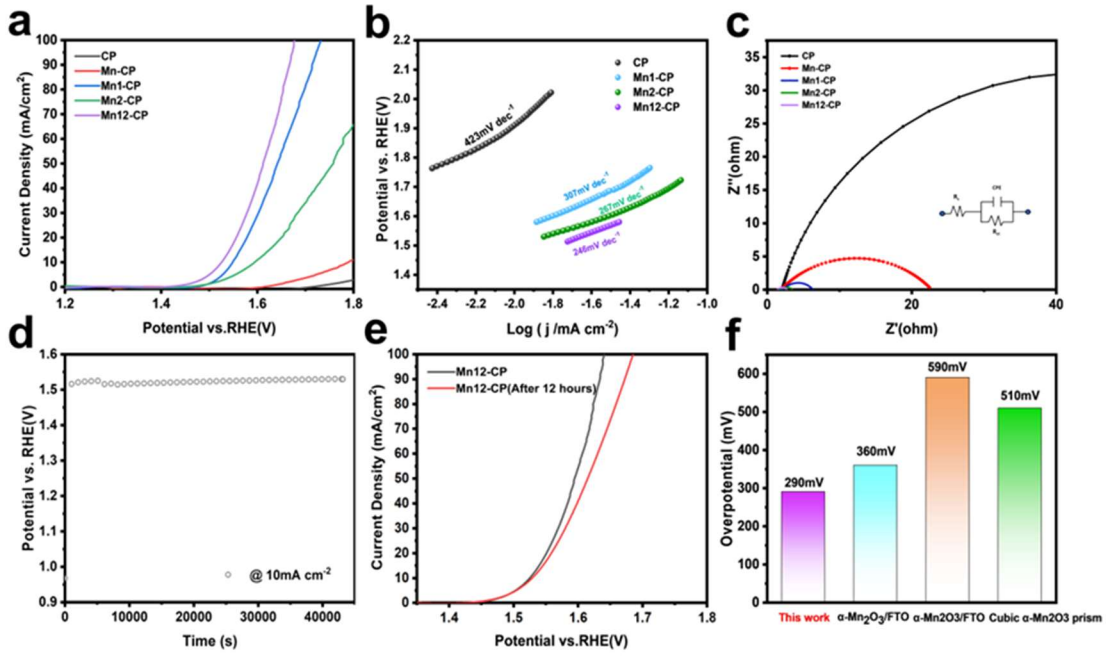

Figure 4. (a) LSV diagram of Mn1-CP with Mn2-CP and Mn12-CP with CP, (b) Tafel diagram of Mn1-CP with Mn2-CP and Mn12-CP, (c) Electrochemical impedance spectroscopy (EIS), (d) This material is stable for 12 hours, (e) comparison of LSV diagram after stability at 12. (f) comparison of overpotential.

The OER performance of Mn12-CP was evaluated in a three-electrode system with an IM KOH solution (pH = 13.7) as the electrolyte. Electrochemical OER properties of blank carbon paper, Mn1-CP, and Mn2-CP were also measured for comparison. Figure 5a shows the LSV curves for all electrocatalysts, Overpotential at current density of 10 mA cm−2 (η10) for Mn12-CP is 290 mV. Figure 4b demonstrates Tafel slopes of the Mn12-CP, showing that their Tafel slopes are 246 mV dec−1, which is smaller than those of the Mn1-CP (307 mV dec−1), Mn2-CP (267 mV dec−1) and CP (423 mV dec−1). Electrochemical impedance spectroscopy (EIS) was performed and fitted using an equivalent circuit with electrolyte resistance (Rs), charge transfer resistance (Rct), and a constant phase element (Figure 5c). The electrochemically active surface area (ECSA), a measure of catalytic activity, is detailed in Figures S5 and S6. The long-term durability during electrolysis was evaluated in a 1M KOH solution using chronopotentiometry. As

ISSN: 2710-0723

depicted in Figure 5d and Figure 5e, stability was maintained at 10mA for 12 hours and at 1.5V when referenced to a standard hydrogen electrode (vs. RHE). This finding comprehensively demonstrates the stability of the manganese-based oxide under alkaline conditions. Moreover, the performance only exhibits slight degradation after the 12-hour test, highlighting its stability and effective oxygen evolution reaction performance. Among the existing catalysts of manganese-based oxides, this work has the lowest Overpotential in Figure 5f[13,14].

4. Conclusion

Constant voltage anodic deposition is a simple and effective method for preparing uniform manganese oxide films. It was discovered that annealing at 300℃ resulted in the formation of Mn1-CP(Mn2O3), whereas annealing at 500℃ led to the formation of Mn2-CP (α-MnO2). The combination of both on the Mn2-CP oxide film covering a layer of Mn1-CP oxide film forms a new synthesized hybrid manganese-based oxides, enhancing its chemical performance and it has good stability. The discovery that Mn2-CP can lower its onset potential implies that Mn2-CP can further enhance its conductivity, thereby reducing its OER overpotential. The combination of the two manganese oxides exhibits optimal performance. This study not only offers a novel perspective on the application of manganese oxides in the alkaline oxygen evolution reaction but also expands their applicability in oxygen evolution reactions more broadly.

Acknowledgments

Natural Science Foundation.

References

[1] M.K. Debe, Nature 486 (2012) 43–51.
[2] S. Guo, S. Zhang, S. Sun, Angewandte Chemie - International Edition 52 (2013) 8526–8544.
[3] R.R. Rao, M.J. Kolb, N.B. Halck, et al., Energy Environ Sci 10 (2017) 2626–2637.
[4] L.C. Seitz, C.F. Dickens, K. Nishio, et al., A highly active and stable IrO x /SrIrO 3 catalyst for the oxygen evolution reaction, n.d. https://www.science.org.
[5] W. Shi, W.S.V. Lee, J. Xue, ChemSusChem 14 (2021) 1634–1658.
[6] K.K. Hazarika, C. Goswami, H. Saikia, et al., Molecular Catalysis 451 (2018) 153–160.
[7] N. Parveen, S.A. Ansari, M.Z. Ansari, et al., Environ Chem Lett 20 (2022) 283–309.
[8] A. Dhiman, D.G. Ivey, Batter Supercaps 3 (2020) 293–305.
[9] M. Kölbach, S. Fiechter, R. van de Krol, et al., Catal Today 290 (2017) 2–9.
[10] P.P. Liu, Y.Q. Zheng, H.L. Zhu, et al., ACS Appl Nano Mater 2 (2019) 744–749.
[11] Y. Liu, N. Ran, R. Ge, et al., Chemical Engineering Journal 425 (2021).
[12] E.S. Ilton, J.E. Post, P.J. Heaney, et al., Appl Surf Sci 366 (2016) 475–485.
[13] M. Jahan, S. Tominaka, J. Henzie, Dalton Transactions 45 (2016) 18494–18501.
[14] Y. Zhou, P. Guan, F. Chen, et al., J Colloid Interface Sci 642 (2023) 23–28.